Terminal middle Pleistocene eruptions of Changbaishan-Tianchi volcano in northeast China: Triggered by the glacial/interglacial climatic transition?

Bo Pan[1,1], Jiandong Xu[2,2], Tanzhuo Liu[3,3], Jingwei Zhang[2,2], Bingrui Zhou[2,2], and Guangpei Zhong[4,4]

[1]Institute of Geology, CEA
[2]Institute of Geology, China Earthquake Administration
[3]Columbia University
[4]Changbaishan Volcano Observation

January 20, 2023

Abstract

High-resolution $^{40}Ar/^{39}Ar$ dating of Bingchang (BC) eruptions of Changbaishan-Tianchi volcano in NE China yields an oldest plateau age of 137.7 ka, well coinciding with the onset of the Penultimate Deglaciation (PDG). Subsequent eruptions occurred at 132.5-131.7 and 124.2 ka during the PDG and the early phase of the Last Interglacial. The BC tephra in marine sediments from the Japan Sea was deposited during the glacial/interglacial climatic transition. These findings suggest that the BC eruptions were likely triggered by depressurization of the volcano's magma chamber through mountain glacial melting/retreat during the early phase of the PDG. The peak timing of the Penultimate Glacial Maximum thus derived falls between 142.7-137.7 ka, closely tied to the time of maximum global ice volume/sea level drop at ˜140 ka. Since the BC tephra is widely dispersed in marine sediments in the Japan Sea, it will serve as a new well-dated stratigraphic marker for the region.

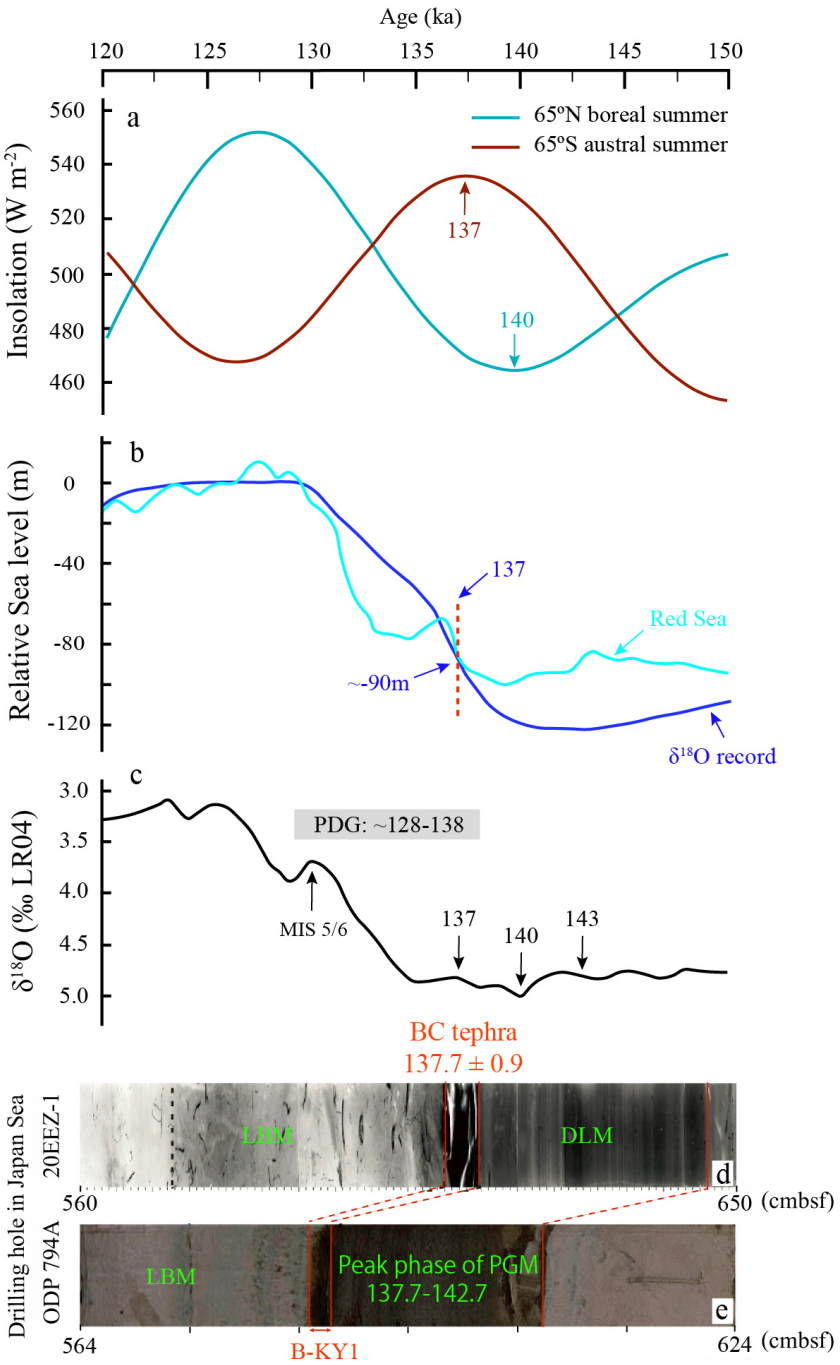

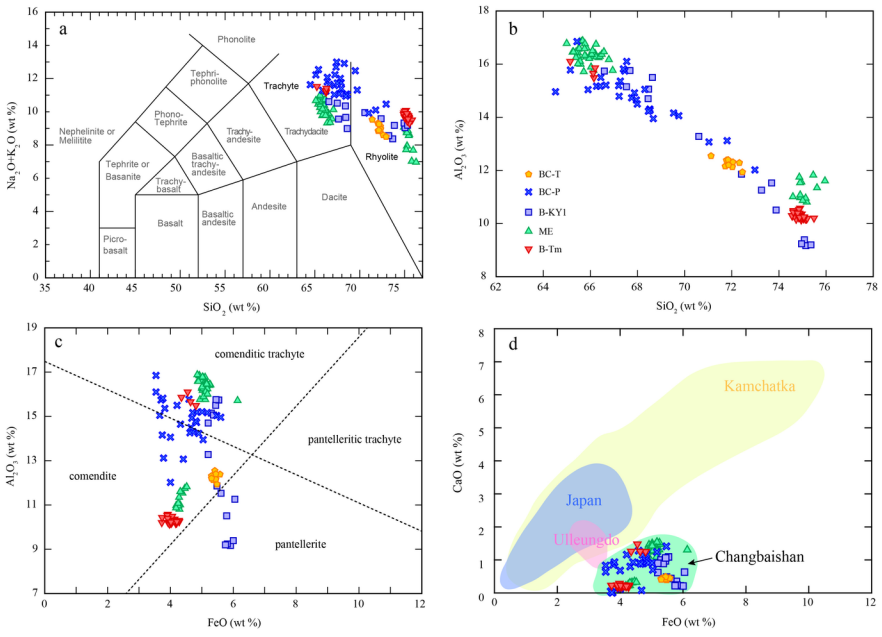

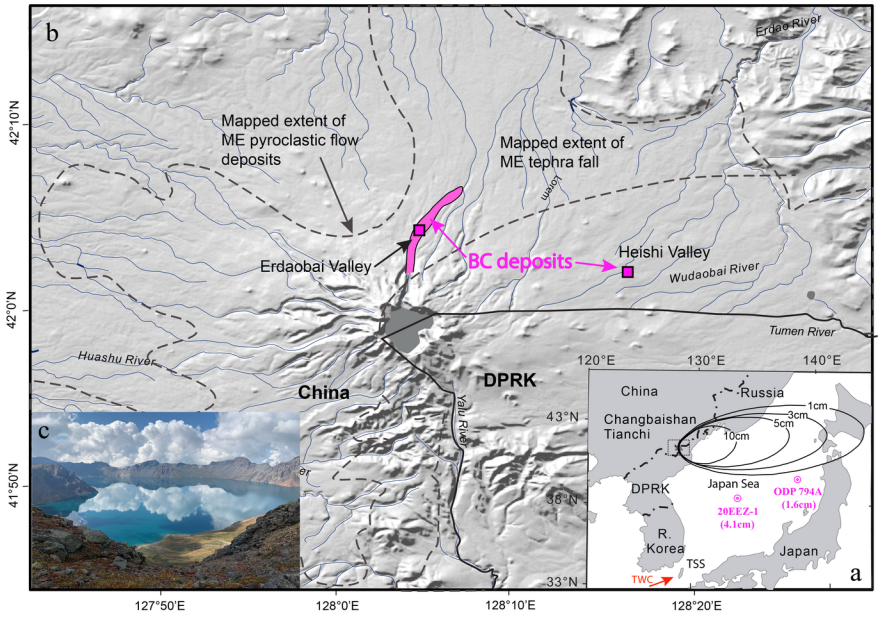

Terminal middle Pleistocene eruptions of Changbaishan-Tianchi volcano in northeast China: Triggered by the glacial/interglacial climatic transition?

Bo Pan[1,2*], Jiandong Xu[1,2], Tanzhuo Liu[2,3], Jingwei Zhang[1,2], Bingrui Zhou[1,2], and Guangpei Zhong[1,4]

1. Jilin Changbaishan Volcano National Observation and Research Station, Institute of Geology, China Earthquake Administration (CEA), Beijing, China
2. CEA Key Laboratory of Seismic and Volcanic Hazards, Beijing, China
3. Lamont-Doherty Earth Observatory of Columbia University, Palisades, New York, USA
4. Changbaishan Volcano Observation, Antu, Jilin, China

Key Points

- Bingchang eruptions took place around 137.7-124.2 ka
- Bingchang eruptions were likely triggered by the Penultimate Deglaciation
- The peak timing of the Penultimate Glacial Maximum dated to 142.7-137.7 ka

Abstract

High-resolution $^{40}Ar/^{39}Ar$ dating of Bingchang (BC) eruptions of Changbaishan-Tianchi volcano in NE China yields an oldest plateau age of 137.7 ka, well coinciding with the onset of the Penultimate Deglaciation (PDG). Subsequent eruptions occurred at 132.5-131.7 and 124.2 ka during the PDG and the early phase of the Last Interglacial. The BC tephra in marine sediments from the Japan Sea was deposited during the glacial/interglacial climatic transition. These findings suggest that the BC eruptions were likely triggered by depressurization of the volcano's magma chamber through mountain glacial melting/retreat during the early phase of the PDG. The peak timing of the Penultimate Glacial Maximum thus derived falls between 142.7-137.7 ka, closely tied to the time of maximum global ice volume/sea level drop at ~140 ka. Since the BC tephra is widely dispersed in marine sediments in the Japan Sea, it will serve as a new well-dated stratigraphic marker for the region.

Plain Language Summary

Changbaishan-Tianchi volcano is a major active stratovolcano in northeast China. It had an episode of explosive Bingchang (BC) eruptions that might have been triggered by major climate changes during the terminal middle Pleistocene. High-resolution radiometric dating of the volcanics indicates that the BC eruptions took place around 137.7-124.2 ka. The distal tephra deposits of these eruptions are linked to the previously-identified B-KY1 tephra in marine sediment cores from the Japan Sea, which was deposited during the penultimate glacial/interglacial transition. Our findings suggest that the BC eruptions were likely triggered by depressurization of the magma reservoirs of the volcano due to glacial melting and retreat during the early phase of the Penultimate Deglaciation (~138-128 ka). This study also yields new well-dated age constraints of 142.7-137.7 ka for the peak timing and duration of the Penultimate Glaciation.

Keywords: Bingchang eruption; B-KY1 tephra; magma chamber depressurization; glacial/interglacial climatic transition; Penultimate Glacial Maximum.

1. Introduction

The Changbaishan-Tianchi volcano (CBS-TC; 42°01`N/128°03`E) is a major active stratovolcano located at the border region between China and Democratic People's Republic of Korea (DPRK) (Figure 1). It is well known for its 946-947 CE Millennium Eruption (ME) and has been of intensive research focus following its 2002-2005 unrest episode (Pan et al., 2017; Xu et al., 2012). Volcanic activities at CBS-TC began around ~22 Ma with widespread basaltic shield-building basaltic magmas. Cone-formation started at ~1 Ma with magmatic compositions ranging from trachytic to peralkaline rhyolitic. Multiple Plinian eruptions during the late Pleistocene are considered to be responsible for the formation of the summit caldera (Wei et al., 2013). The ME was the last major eruption of this volcano (VEI 6.2-7.0) (Oppenheimer, 2017; Yang et al., 2021), with distal tephra deposits (B-Tm) identified in marine sediment cores from the Japan Sea and Hokkaido, Japan (Chen et al., 2016) (Figure 1). Various Cenozoic explosive eruptions prior to the ME have been identified but still remain poorly studied (Jin & Zhang, 1994; Liu et al., 2008).

Here we report a proximal suite of grey tephra and black tuff along Heishi Valley (HSV) and Erdaobai Valley (EBV) in the CBS-TC volcanic field (Figure 1). High-resolution $^{40}Ar/^{39}Ar$ dating of the volcanics indicates that they were produced during the Bingchang (BC) eruptions around 137-124 ka. Electron microprobe analyses of the BC eruptives reveal that their chemical compositions closely match that of the B-KY1 tephra in marine sediment cores from the Japan Sea, which was deposited at the boundary of Marine Isotope Stage (MIS) 6/5 during the glacial/interglacial climatic transition (Chun et al., 2006; Chun & Cheong, 2020). These findings suggest that the BC eruptions were likely triggered by depressurization of the volcano's magma chamber through mountain glacier melting and retreat during the early phase of the Penultimate Deglaciation (PDG, ~138-128 ka) (Menviel et al., 2019). Furthermore, the $^{40}Ar/^{39}Ar$-dated BC/B-KY1 tephra yields new age constraints of 142.7-137.7 ka on the peak timing and duration of the Penultimate Glacial Maximum (PGM) recorded in the marine sediment cores, which substantiate the LR04-based chronology of the PGM (Lisiecki & Raymo, 2005; Menviel et al., 2019).

2. The BC eruptions and the B-KY1 tephra layer

The proximal products of the BC eruptions were first described by Jin and Zhang (1994). These eruptives outcrop mainly as tephra fall (BC-T) in HSV and as pyroclastic deposit (BC-P) in EBV

(Figure 1). BC-T is ~2 m thick and composed of white to grey pumice at the bottom and pale-yellow pumice at the top (Figure S1) with abundant lithic and crystal fragments. Discrete, juvenile pumice comprises ~80% of the deposit, with a maximum clast size of ~5 cm and modal size of 2-3 cm. Lithic fragments are primarily of trachyte and basalt with a maximum size of ~1 cm. Crystal fragments are primarily of ~1 mm-sized feldspar with minor quartz, pyroxene, and olivine. BC-P is exposed along EBV, with a total thickness of ~200 m (Figure S1). Owing to its proximity to the edifice of the volcano, BC-P is moderately to intensely welded, composed of volcanic ash and deformed clasts (fiamme) with abundant feldspar crystal fragments (~30%). Large lithic fragments up to 10s of cm are observed in BC-P. The eruptive products from the trachytic phase of the ME (ME-Tr, 20-30 m thick) are superficially similar to the BC eruptives here, but they can be distinguished via welding extent and/or $^{40}Ar/^{39}Ar$ dating (Pan et al., 2017).

The B-KY1 tephra layer was first reported in the 20EEZ-1 core (611.5-615.6 cmbsf) and later fully described in the ODP 794A core (585.6-587.2 cmbsf) from the Janpa Sea (Chun et al., 2006; Chun & Cheong, 2020) (Figure 1). It is about 1.6 to 4.1 cm thick in the marine sediment cores and consists of pumice shards, bubble-wall shards, and minor phenocrysts. The compositions of B-KY1 tephra range from alkaline trachyte to sub-alkaline rhyolite, similar to that of B-Tm tephra (Figure 2; Table S1). Moreover, B-KY1 tephra was noted as a sharp boundary layer between the underlying dark laminated mud (DLM) and the overlying light bioturbated mud (LBM) in the marine sediments (Chun & Cheong, 2020; Tamaki et al., 1990). The deposition of both DLM and LBM layers reflects dramatic changes in the regional dynamics of oceanic current systems and bottom water conditions (anoxia vs. oxygenation) associated with the glacial/interglacial climatic transition (Chun & Cheong, 2020; Khim et al., 2007; Saavedra-Pellitero et al., 2019; Tada et al., 2018).

3. Sample collection and age determination

One sample of BC-T was collected from HSV (Figure S1). Loose tephra of size 2-4 cm was manually picked, then rinsed with deionized water in an ultrasonic bath for 30 minutes to remove surface impurities. Four samples of BC-P were collected from the east wall of EBV (i.e., BC-P3 at top and BC-P2 at bottom) and along the river channel (BC-P1L and BC-P1R) (Figure S1). They were cut to remove all surface material. Petrographic thin sections of the samples were prepared by Wagner Petrographic Inc., USA and then studied for textural and mineralogical characteristics.

Major elemental compositions of glass in BC-T (matrix) and BC-P (fiamme) were analyzed using a Cameca SX-100 electron microprobe (EPMA) at Oregon State University (OSU), USA. Sanidine phenocrysts were separated and prepared for $^{40}Ar/^{39}Ar$ dating. The phenocryst grains were irradiated for 1 hour at the OSU TRIGA reactor and then extracted and analyzed using a 25 W Synrad CO_2 laser and an ARGUS VI multi-collector mass spectrometer at the OSU Argon Geochronology Lab. The detailed processes of sample preparation and $^{40}Ar/^{39}Ar$ dating are given in the supporting material.

4. Results

4.1. Petrology and geochemical characteristics of the BC eruptions

BC-T is typically white or light yellow, vesicular (30-40%) with thin vesicle walls, and phenocryst-poor with 5-8 volume% crystals, composed of anorthoclase/Na-sanidine (~80%), Hedenbergite (~10%), fayalitic olivine (~5%), and quartz (~5%). BC-P is black welded tuff with abundant fiamme, and phenocryst-rich with 30-60 volume%, consisting of Na-sanidine (~90%), Hedenbergite (~5%), fayalitic olivine (~3%), and quartz (~2%). The compositions of BC eruptives broadly parallel that of the ME deposits, with BC-T similar to the ME comendite (ME-Com), and BC-P similar to the ME trachyte (ME-Tr) (Pan et al., 2017, 2020). Major element compositions of the BC glass display coherent trends between trachytic and comenditic (Figure 2).

4.2. $^{40}Ar/^{39}Ar$ geochronology of the BC eruptions

One BC-T and four BC-P samples were selected for $^{40}Ar/^{39}Ar$ dating via single-crystal incremental heating (SCIH) (Andersen et al., 2017; Ramos et al., 2016). Four to eight sanidine grains from each sample were measured with 15-17 steps of incremental heating. All analyses yielded uniform plateau ages with increasing laser power, although some show abnormal ages at lower and higher laser power due likely to excess argon (Andersen et al., 2017) (Table S2). For each sample, we report $^{40}Ar/^{39}Ar$ dating results that show a relatively younger weighted plateau age with more released ^{39}Ar gas (>90%) and a smaller MSWD value (Table 1; Figure S2). BC-T tephra sampled from HSV yields the oldest plateau age of 137.7 ± 0.9 ka, and it is therefore interpreted as a marker for the initial phase of the BC eruptions (Table 1). BC-P1L and BC-P1R, sampled from the lower parts of BC-P tuff along EDV, yield intermediate plateau ages of 131.7 ± 1.1 ka and 132.5 ± 0.4 ka, respectively. BC-P2 sampled from the bottom of the east cliff of EDV yields a plateau age of

132.2 ± 1.8 ka. This date overlaps with that of BC-P1L and BC-P1R within the 2σ age range, suggesting that these deposits were mostly likely originated from the same eruption around 131.7-132.5 ka. BC-P3 was collected at top of the east cliff above BC-P2, with a plateau age of 124.2 ± 0.8 ka, making it the youngest known eruption from the BC episode. Figure S3 depicts a cross-sectional distribution of volcanic deposits at EBV, showing BC pyroclastic flow sequences and relevant $^{40}Ar/^{39}Ar$ ages, along with ME-Tr deposits produced in 946-947 CE. These $^{40}Ar/^{39}Ar$ ages gradually decrease from BC-T to BC-P3, systematically corresponding to their positions in the stratigraphic sequence.

5. Discussion

5.1. BC eruptions as the source of the B-KY1 tephra

The relatively low FeO-CaO ratio of glass composition of BC-T tephra enables it to be easily identified among other volcanic eruptives in northeast Asia (Chun & Cheong, 2020; Sun et al. 2018). As illustrated in Figure 2, the proximal BC-T tephra in HSV is dispersed in composition between comenditic and trachytic, and is petrologically and geochemically similar to that of B-KY1 tephra in the Japan Sea. The composition of the BC-P tuff is also broadly consistent with that of B-KY1 but shows a wider dispersion. Furthermore, based on the LR04 benthic $\delta^{18}O$ timescale for the marine sediment core of ODP 794A, the depositional age of B-KY1 tephra was estimated to be around ~135 ka by Chun & Cheong (2020), overlapping with our $^{40}Ar/^{39}Ar$ ages of 137-124 ka for the BC eruptions. Taken together, these pieces of evidence indicate that B-KY1 tephra was most likely sourced from the CBS-TC volcano and thus represents the distal tephra deposit of the BC eruptions at locations about 600-900 km southeast of the summit caldera (Figure 1).

5.2. Climatic change as a possible trigger for the BC eruptions

There is a growing recognition that volcanism can be initiated and/or exacerbated by magma chamber depressurization at its overlying surface during glacier retreating and/or sea level drop (Albino et al., 2010; Cooper et al., 2018; Huybers & Langmuir, 2009; Rampino et al., 1979; Schmidt et al., 2013). For instance, the magmatism of mid-ocean ridges appears to keep pace with changing sea levels and Milankovitch glacial-interglacial cycles (Crowley et al., 2015; Lund & Asimow, 2011). Large variations and increase in eruption rate across Iceland over the past 10,000 years were likely caused by the last deglaciation through ice sheet removal-induced mantle melting

(Jull & McKenzie, 1996). Increased volcanic activities at Santorini, Greece have been associated with >40 m sea level drops over the past 360,000 years (Satow et al., 2021).

The Changbaishan Range consitutes the mountaneous terrains spanning the latitudes of 38°46'-47°30′N and longitudes of 121°08'-134°00'E in northeast China. As the highest peak of the mountain range, the CBS-TC crater is 25-30 km in diameter at its base and rises to an altitude of 2749 m on the caldera rim (Wei et al., 2013) (Figure 1). Regional climate is of temperate continental mountain type influenced by the North Pacific monsoons and the Siberian anticyclone, with mean annual temperature of -7.3°C and annual precipitation of 1342 mm measured near the summit caldera (Shi, 2005). The present-day theoretical snow line is estimated to be around 3380 ± 100 m (Zhang et al., 2008). Although thick snow accumulates during winters and springs, no modern glaciers have developed in the summit areas.

However, large-scale glaciers are known to have developed in the summit areas during the Last Glacial Maximum (LGM; 26-19 ka). Numerous glacial features are well preserved around the caldera and their formation was attributed to the LGM (Shi et al., 2005; Zhang et al., 2008). These include glacial cirques, trough valleys, and glacial striations both inside the caldera and on the crater slopes. The level of cirque floors defines the equilibrium line altitude (ELA) to 2000-2300 m during the LGM, about 1000-1200 m lower than that in the Tianshan Mountains of western China at the same latitude, suggesting that maritime temperate mountain glaciers have covered the crater areas due to increased winter monsoonal precipitation during the LGM (Shi et al., 2005).

During the PGM, the altitude of the CBS-TC crater before the BC eruptions is speculated to be considerably high around 3500-4000 m (Wei et al., 2013), well above the northern hemisphere glacial altitude of ~2300 m in the regions around 40-42°N latitudes (Evan & Cox, 2005). Therefore, the crater and its surrounding areas were likely heavily glaciated during the PGM. Since the PGM was much severer and more protracted than the LGM over Eurasia (Colleoni et al., 2016; Svendsen et al., 2004), the overlying glaciers and snow/ice cover on the pre-BC crater were presumably much thicker than during the LGM, imposing large gravitational load-induced pressure on the underlying magma chamber. Furthermore, seismic tomographic studies of the volcano (Zhao et al., 2009; Zhu et al., 2019) indicate that its formation is related to the upwelling of hot and wet asthenospheric materials in the big mantle wedge above the stagnant Pacific slab and was likely caused by plate tectonic processes in the upper mantle. The crustal magma chamber

of the volcano, about 5-15 km below the ground surface (Xu et al., 2012), accumulated highly-evolved and volatile-rich magma and thus attained an excessively high pressure condition during the terminal phase of the PGM. Following the onset of the PDG at ~137-138 ka (Clark et al., 2020) (Figure 3c) and as an early response to the deglacial climate change due to the crater's relatively lower latitude (42°N), mountain glaciers and snow/ice cover were rapidly reduced or completely removed from the pre-BC crater and surrounding regions, which likely induced depressurization of the crustal magma chamber. The deglaciation also led to increased melting in the upper mantle which supplied the more primitive basaltic melts to the shallow reservoirs for imminent eruptions (Cooper et al., 2018; Iacovino et al., 2016; Pan et al., 2017). Such a glacial/interglacial climatic transition is speculated to serve as a possible trigger for the BC eruptions.

Evidence from the marine sediment cores in the Japan Sea appears to support this scenario. During the terminal phase of the PGM, the global sea level dropped below -90 to -120 m (Bintanja et al., 2005; Grant et al., 2014; Menviel et al., 2019) (Figure 3b), which caused the near closure of the Tsushima Strait (TSS) and the cessation of Tsushima Warm Current (TWC) into the Japan Sea (Gorbarenko & Southon, 2000; Khim et al., 2007; Tada & Irino, 1999; Tada et al., 2018) (Figure 1a). As a result, the Japan Sea became a large isolated and stratified water body facilitating the condition of bottom water anoxia (Khim et al., 2007; Tada et al., 2018). In the ODP 794A, 20EEZ-1 and other marine sediment cores, the deposition of the stratigraphically lower DLM layer reflects bottom water anoxia during the terminal phase of the PGM (Chun & Cheong, 2020; Khim et al., 2007; Tada et al., 2018). An upward transition to the LBM layer reflects bottom water oxygenation generated by restored oceanic circulations through the reopening of the Japan Sea to the Pacific during the PDG (Chun & Cheong, 2020; Khim et al., 2007; Tada et al., 2018). The B-KY1 tephra layer in the marine sediment cores was deposited between the underlying DLM and the overlying LBM layers (Figure 3d, e), suggesting that the BC eruptions were concurrent with and therefore likely triggered by the glacial/interglacial climatic transition.

5.3. Implication for the peak timing and duration of the PGM

The PGM often refers to the maximum advance of the Eurasian ice sheet around ~160-140 ka (Colleoni et al., 2016; Svendsen et al., 2004). In the LR04 benthic $\delta^{18}O$ stack record, the peak phase of the PGM is characterized by the deepest trough of the $\delta^{18}O$ curve interpreted to represent the interval of maximum global sea level drop and (inversely) global ice volume during MIS 6

(Grant et al., 2014; Lisiecki & Raymo, 2005; Menviel et al., 2019). Based on the LR04 age model, the peak timing of the PGM is centered at 140 ka, with a duration of 6 kyr from 143 to 137 ka (Figure 3c). U/Th dating of Tahitian fossil corals (Thomas et al., 2009) indicates sea level rise to -85 m and an inception of the PDG by 137 ka. Transient climate simulations (Clark et al., 2020) further show that both the Greenland and the Antarctic Ice Sheets start to deglaciate from their PGM extents at ~137.5 ka. These age data are consistent with the LR04-based chronology of the PGM (Figure 3c). $^{40}Ar/^{39}Ar$ dating of BC/B-KY1 tephra from this study yields new age constraints on the peak timing and duration of the PGM that substantiate the LR04-based chronology, as discussed below.

In the Japan Sea, the DLM layer overlain by the $^{40}Ar/^{39}Ar$ dated BC/B-KY1 tephra at the ODP 794A site was deposited at the depth interval of 606.2 to 587.2 cmbsf, with a sedimentation rate of ~3.5 cm/kyr estimated for the top core section of the hole (0-2550 cmbsf) (Tamaki et al., 1990). This sedimentation rate is however too crude to be used for accurate age estimating of marker layers in the core due to its large temporal variations (Chun & Cheong, 2020; Tamaki et al., 1990). During IODP Expedition 346, hole U1424A was dilled at a site about 600 m east of the 794A site. The DLM layer identified as marker layer "2-1" at the depth interval of 607.2-587.2 cmbsf is stratigraphically correlated with the DLM layer at the 794A site, and their deposition was interpretated to reflect a period of bottom water anoxia associated with the terminal phase of the PGM when the global sea level dropped below -90 m (Chun & Cheong, 2020; Tada et al., 2018).

Based on the LR04-tuned high-resolution age model of hole U1424A, the linear sedimentation rate (LSR) of the core section (607.2-485 cmbsf) that contains DLM layer "2-1" is 3.759 cm/kyr (Tada et al., 2018). Given the short distance of ~600 m between the two sites, the same sedimentation rate of 3.759 cm/kyr is thus assumed for the deposition of the DLM layer at the 794A site. Assigning the $^{40}Ar/^{39}Ar$ age of 137.7 ka to the top of this DLM layer (19 cm in thickness), we estimate an age of 142.7 ka for its base. These new age constraints bracket a depositional time interval of 5 kyr for the DLM layer, corresponding to the duration of the peak phase of the PGM from 142.7 to 137.7 ka recorded in the marine sediments. The mean age of 140.2 ka for the DLM layer is closely tied to the peak timing of the PGM at 140 ka (Lisiecki & Raymo, 2005) (Figure 3c). The 5-6 kyr duration of the peak phase of the PGM is also comparable to the 6-7 kyr duration of the LGM (26.5-19 to 20 ka) (Clark et al., 2009), which may yield new insights into the ice-sheet

formation and dynamics during past glacial-interglacial cycles (Clark et al., 2020; Colleoni et al., 2016; Hughes & Gibbard, 2019; Rohling et al., 2017).

6. Conclusion

The BC eruptive episode of the CBS-TC volcano took place in the terminal middle Pleistocene around 137.7-124.2 ka. The distal tephra deposits of these eruptions are linked to the previously-identified B-KY1 tephra in the marine sediment cores from the Japan Sea, which marks the MIS 6/5 boundary associated with the glacial/interglacial climatic transition. Our findings suggest that the BC eruptions were likely triggered by depressurization of the magma reservoirs of the volcano due to glacial melting and retreat during the early phase of the PDG. In addition, this study provides new absolutely dated age constraints of 142.7-137.7 ka for the peak timing and duration of the PGM recorded as DLM layers in the marine sediments. Since the BC tephra is widely dispersed in marine sediments in the Japan Sea, it will serve as a new well-dated stratigraphic marker for the region.

Acknowledgements

This research was supported by the National Natural Science Foundation of China (grants nos. 41872254 and 41911540472). We thank Frank Tepley for providing assistance with EMPA, and Daniel Miggins with $^{40}Ar/^{39}Ar$ dating. We also appreciate the cooperation and assistance of the Changbaishan National Park.

Data Availability Statement

The geochemical and geochronological raw data of the BC eruptions are available at the following data repository: https://doi.org/10.5281/zenodo.6658808.

References

Albino, F., Pinel, V., & Sigmundsson, F. (2010). Influence of surface load varistions on eruption likelihood: application to two Icelandic subglacial volcanoes, Grimsvon and Katla. *Geophysical Journal International, 181(3),* 1510-1524.

Andersen, N., Jicha, B. R., Singer, B. S., & Hildreth, W. (2017). Incremental heating of Bishop Tuff sanidine reveals preeruptive radiogenic Ar and rapid remobilization from cold storage. *PNAS, 114(47),* 12407-12412.

Bintanja, R., Roderik, S. W., Wal, V. & Oerlemans, J. (2005). Modelled atmospheric temperatures and global sea levels over the past million years. *Nature, 437,* 125-128.

Chen, X. Y., Blockley, S. P. E., Tarasov, P. E., Xu, Y. G., McLean, D., Romlinson, E. L., et al. (2016). Clarifying the distal to proximal tephrochronology of the Millennium (B-Tm) eruption, Changbaishan Volcano, northeast China. *Quaternary Geochronology, 33,* 61-75.

Chun, J. H., & Cheong, D. (2020). Origin of compositional diversity of marine tephra during the Late Middle Pleistocene B-KY1 Baekdusan volcanic eruption. *Applied Sciences, 10*, L4469.

Chun, J. H., Cheong, D., Han, S. J., Hub, S., & Yoo, H. S. (2006). Tephrostratigraphy and paleoenironments of marine core in the Kita-Yamato trough, East Sea/Japan Sea. *Economic and Environmental Geology, 39*, 83-93.

Clark, P. U., Dyke, A. S., Shakun, J. D., Carlson, A. E., Clark, J., Wohlfarth B., et al. (2009). The Last Glacial Maximum. *Science, 325*, 710-714.

Clark, P. U., He, F., Golledge, N. R., Mitrovica, J. X., Dutton, A., Hoffman, J. S., et al. (2020). Oceanic forcing of penultimate deglacial and last interglacial sea-level rise. *Nature, 577*, 660-664.

Colleoni, F., Wekerle, C., Naslund, J. O., Brandefelt, J., & Masina, S. (2016). Constraint on the penultimate glacial maximum Northern Hemisphere ice topography. *Quaternary Science Reviews, 137*, 97-112.

Cooper, C. L., Swindles, G. T., Savov, I. P., Schmidt, A., & Bacon, K. L. (2018). Evaluating the relationship between climate change and volcanism. *Earth-Science Reviews, 177*, 238-247.

Crowley, J. W., Katz, R. F., Huybers, P., Langmuir, C. H., & Park, S. H. (2015). Glacial cycles drive variations in the production of oceanic crust. *Science, 347*, L1261508.

Evans, I. S., & Cox, N. J. (2005). Global variations of local asymmetry in glacier altitude: separation of north–south and east–west components. *Journal of Glaciology, 51(74),* 469-482.

Gorbarenko, S.A., & Southon, J.R., 2000, Detailed Japan Sea paleoceanography during the last 25 kyr: constraints from AMS dating and $\delta^{18}O$ of planktonic foraminifera: *Palaeogeography, Palaeoclimatology, Palaeoecology, 156*, 177-193.

Grant, K. M., Rohling, E. J., Ramsey, C. B., Cheng, H., Edwards, R. L., Florindo, F., et al. (2014). Sea-level variability over five glacial cycles. *Nature Communications, 5*, 5076.

Horn, H., & Schmincke, H.U. (2000). Volatile emission during the eruption of Baitoushan volcano (China/North Korea) ca. 969 AD. *Bulletin of Volcanology, 62*, 537-555.

Hughes, P., & Gibbard, P. (2019). Global glacier dynamics during 100 ka Pleistocene glacial cycles. *Quaternary Research, 90*, 222–243.

Huybers, P., & Langmuir, C. (2009). Feedback between deglaciation, volcanism, and atmospheric CO_2. *Earth and Planetary Science Letters, 286*, 479-491.

Iacovino K., Song K. J., Sisson T., Lowenstern, J., Ri, K. K., Jang, J. N., et al. (2016). Quantifying gas emissions from the "Millennium eruption" of Paektu volcano, Democratic People's Republic of Korea/China. *Science Advances, 2*, e1600913.

Jin, B. L., & Zhang, X. Y. (1994). Research on volcanic Geology in Changbaishan, Yanji, Yanbian Northeast Korean Nationality Education Press.

Jull, M., & McKenzie, D. (1996). The effect of deglaciation on mantle melting beneath Iceland. *Journal of Geophysical Research, 101*, 21815-21828.

Khim, B. K., Hahk, J. J., Hyun, S., & Lee, G. H. (2007). Late Pleistocene dark laminated mud layers from the Korea Plateau, western East Sea/Japan Sea, and their paleoceanographic implications. *Palaeogeography, Palaeoclimatology, Palaeoecology, 247*, 74-87.

Laskar, J., Robutel, P., Joutel, F., Gastineau, M., Correia, A. C. M., & Levrard, B. (2004). A long-term numerical solution for the insolation quantities of the Earth. *Astronomy & Astrophysics, 428*, 261-285.

Lisiecki, L. E., & Raymo, M. E. (2005). A Pliocene-Pleistocene stack of 57 globally distributed benthic $\delta^{18}O$ records. *Paleoceanography, 20*, PA1003.

Liu, Q., Pan, X. D., Wei, H. Q., Yun, S. H., Sun, C. Q., & Jin, B. L. (2008). A borehole study on the eruptive sequence from the Tianchi volcano, Changbai Mountain. *Earthquake Research in China, 24(3),* 235-246.

Lund, D. C., & Asimow, P. D. (2011). Does sea level influence mid-ocean ridge magmatism on Milankovitch timescales, Geochemistry, *Geophysics, Geosystems, 12*, L12009.

McLean, D., Albert, P., Nakagawa, T., Suzuki, T., Staff, R. A., Yamada, K. (2018). Integrating the Holocene tephrostratigraphy for East Asia using a high-resolution cryptotephra study from Lake Suigetsu (SG14 core), central Japan. *Quaternary Science Reviews, 183*, 36–58.

Menviel, L., Capron, E., Govin, A., Dutton, A., Tarasov, L., Ouchi, A. A., et al. (2019). The penultimate deglaciation: protocol for Paleoclimate Modelling Intercomparison Project (PMIP) phase 4 transient numerical simulations between 140 and 127 ka, version 1.0. *Geoscientific Model Development, 12*, 3649-3685.

Oppenheimer, C., Wacker, L., Xu, J. D., Galvan, J. D., Stoffel, M., Guillet, S., et al. (2017). Multi-proxy dating the 'Millennium Eruption' of Changbaishan to late 946 CE. *Quaternary Science Reviews, 158*, 164-171.

Pan, B., de Silva, S. L., Xu, J. D., Chen, Z. Q., Miggins, D. P., & Wei, H. Q. (2017). The VEI-7 Millennium eruption, Changbaishan-Tianchi volcano, China/DPRK: New field, petrological, and chemical constraints on stratigraphy, volcanology, and magma dynamics. *Journal of Volcanology and Geothermal Research, 343,* 45-59.

Pan, B., de Silva, S. L., Xu, J. D., Liu, S. J., & Xu, D. (2020). Late Pleistocene to present day eruptive history of the Changbaishan-Tianchi Volcano, China/DPRK: New field, geochronological and chemical constraints. *Journal of Volcanology and Geothermal Research, 399*, L106870.

Ramos, F. C., Heizler M. T., Buettner J. E., Gill, J. B., Wei, H. Q., Dimond, C. A., et al. (2016). U-series and $^{40}Ar/^{39}Ar$ ages of Holocene volcanic rocks at Changbaishan volcano, China. *Geology, 44 (7)*, 511–514.

Rampino, M. R., Self, S., & Fairbridge, R. W. (1979). Can rapid climatic change cause volcanic eruptions. *Science, 206*, 826-829.

Rohling, E. J., Hibbert, F. D., Williams, F. H., Grant, K. M., Marino, G., Foster, G. L., et al. (2017). Differences between the last two glacial maxima and implications for ice-sheet, $\delta^{18}O$, and sea-level reconstructions. *Quaternary Science Reviews, 176*, 1-28.

Saavedra-Pellitero, M., Baumann, K. H., Gallagher, S. J., Sagawa, T., & Tada, R. (2019). Paleoceanographic evolution of Japan Sea over the last 460 kyr – A coccolithophore perspective. *Marine Micropaleontology, 152*, L101720.

Satow, C., Gudmundsson, A., Gertisser, R., Ramsey, C. B., Bazargan, M., Pyle, D. M., et al. (2021). Eruptive activity of the Santorini Volcano controlled by sea-level rise and fall. *Nature Geoscience, 14*, 586-592.

Schmidt, P., Lund, B., Hieronymus, C., Maclennan, J., Arnadottir, J., & Pagli, C. (2013). Effects of present-day deglaciation in Iceland on mantle melt production rates. *Journal of Geophysical Research - Solid Earth, 118*(7), 3366-3379.

Shi, Y. F., Cui, Z. J., & Su, Z. (2005). The Quaternary Glaciations and Environmental variations in China. Shijiazhuang, Heibei Science and Technology Publishing House.

Sun, C. Q., Wang, L., Plunkett, G., You, H. T., Zhu, Z. Y., Zhang, L., et al. (2018). Ash from the Changbaishan Qixiangzhan Eruption: A new early Holocene marker horizon across East Asia. *Journal of Geophysical Research - Solid Earth, 123*, 6442-6450.

Svendsen, J., Alexanderson, H., Astakhov, V., Demidov, I., Dowdeswell, J. A., Funder, S., et al. (2004). Late Quaternary ice sheet history of northern Eurasia. *Quaternary Science Reviews, 23*, 1229–1271.

Tada, R., & Irino, T. (1999). Land-ocean linkages over orbital and millennial timescales recorded in late Quaternary sediments of the Japan Sea. *Paleoceanography, 14*(2), 236-247.

Tada, R., Irino, T., Ikehara, K., Karasuda, A., Sugisaki, S., Xuan, C., et al. (2018). High-resolution and high-precision correlation of dark and light layers in the Quaternary hemipelagic sediments of the Japan Sea recovered during IODP Expedition 346. *Progress in Earth and Planetary Science, 5*, L19.

Tamaki, K., Pisciotto, K., Allan, J., et al. (1990). SITE 794. In Proceedings of the Ocean Drilling Program, Initial Reports; in Stewart, N.J., Winkler, W.R., Eds.; Ocean Drilling Program Texas A&M University: College Station, TX, USA, 127, 71–167.

Thomas, A. L., Henderson, G. M., Deschamps, P., Yokoyama, Y., Mason, A. J., Bard, E., et al. (2009). Penultimate deglacial sea-level timing from Uranium/Thorium dating of Tahitian Corals. *Science, 324*, 1186-1189.

Wei, H. Q., Liu, G. M., & Gill, J. (2013). Review of eruptive activity at Tianchi volcano, Changbaishan, northeast China: implications for possible future eruptions. *Bulletin of Volcanology, 75*, L706.

Xu, J.D., Liu, G.M., Wu, J.P., Ming, Y. H., Wang, Q. L., Cui, D. X., et al. (2012). Recent unrest of Changbaishan volcano, northeast China: A precursor of future eruption. *Geophysical Research Letters, 39*, L16305.

Xu, J. D., Pan, B., Liu, T. Z., Hajdas, I., Zhao, B., Yu, H. M., et al. (2013). Climatic impact of the Millennium eruption of Changbaishan volcano in China: new insights from high-precision radiocarbon wiggle-match dating. *Geophysical Research Letters 40,* 54–59. https://doi.org/10.1029/2012GL054246.

Yang, Q. Y., Jenkins, S., Lerner, G., Li, W. R., Suzuki, T., McLean, D., et al. (2021). The Millennium Eruption of Changbaishan Tianchi Volcano is VEI 6, not 7. *Bulletin of Volcanology, 83(11),* L74.

Zhang, W., Niu, Y. B., Yan, L., Cui, Z. J., Li, C. C., & Mu, K. H. (2008). Late Pleistocene glaciation of the Changbai Mountains in northeastern China. *Chinese Science Bulletin, 53(17),* 2672-2684.

Zhao, D. P., Tian, Y., Lei, J. S., Liu, L., & Zheng, S. H. (2009). Seismic image and origin of the Changbai intraplate volcano in East Asia: Role of big mantle wedge above the stagnant Pacific slab. *Physics of the Earth and Planetary Interiors, 173*, 197–206.

Zhu, H., Tian, Y., Zhao, D., Li, H., & Liu, C. (2019). Seismic structure of the Changbai intraplate volcano in NE China from joint inversion of ambient noise and receiver functions. *Journal of Geophysical Research - Solid Earth, 124*, 4984–5002.

Figure Captions

Figure 1. Spatial distribution of BC eruption deposits in Changbaishan-Tianchi (CBS-TC) volcanic field. (a) Location map showing the CBS-TC volcano and marine sediment core sites of 20EEZ-1 and ODP 794A in the Japan Sea. Also shown are the isopach of the Millennium Eruption (ME) tephra (B-Tm) (Horn & Schmincke, 2000) and the thicknesses of BC/B-KY1 tephra (numbers in red) (Chun & Cheong, 2020). (b) Distribution of BC tephra in HSV and pyroclastic flows in EBV. (c) Inset photo showing the modern Tianchi caldera (view west). TSS: Tsushima Strait, deepest point at -130 m. TWC: Tsushima Warm Current. The cessation of TWC into the Japan Sea occurred when global sea level dropped below -90 m during past glacial-interglacial cycles (Tada et al., 2018).

Figure 2. Plots of major element compositions of glass by EPMA in wt% (normalized to 100% anhydrous), with known ranges of compositions from CBS-TC and nearby volcanic systems (Sun et al., 2018). Note that glass compositions of BC-T/BC-P and ME (Pan et al., 2017, 2020; this study) closely match that of B-KY1 and B-Tm in the Japan Sea (Chen et al., 2016; Chun & Cheong, 2020; Chun et al., 2006; McLean et al., 2018), respectively, confirming their shared origin from the CBS-TC volcano. The probe data are given in Table S1.

Figure 3. Proxies of global climate changes and sea-level fluctuations compared with the BC eruptions during the penultimate glacial/interglacial climatic transition. (a) Local summer insolation at 65°N & 65°S (Laskar et al., 2004). (b) Global sea-level reconstructions from ice sheet model and Red Sea relative sea level data (Bintanjia et al., 2005; Menviel et al., 2019). (c) LR04 benthic $\delta^{18}O$ stack curve (Lisiecki & Raymo, 2005). (d, e) X-ray radiographs of cores 20EEZ-1 & ODP 794A showing B-KY1 tephra layer between the underlying dark laminated mud (DLM) and the overlying light bioturbated mud (LBM). Radiographs are taken from Chun & Cheong (2020).

Table Captions

Table 1. $^{40}Ar/^{39}Ar$ ages of BC-T and BC-P deposits from the BC eruptions.

Supporting materials

SAMPLE PREPARATION AND ANALYSES

Over 100 sites around the volcano on the Chinese side of the border areas have been described over decades of study. We recognized that the deposits of the Bingchang (BC) episode are exposed in Heishigou Valley (HSV) and Erdaobai Valley (EBV). We collected samples of BC-T at HSV and BC-P at EBV. All loose BC-T samples were thoroughly rinsed with deionized water in an ultrasonic bath for 30 min to remove surface contaminants, while the exposed surfaces of BC-P samples were cut off entirely. All samples were then dried in an oven for 24 hours. Each sample was divided to be prepared for thin sectioning, epoxy mounts for probe microanalysis, and age determination.

Geochemistry

15 polished thin-sections from BC-T and BC-P were prepared by Wagner Petrographic, USA. Major compositions of glass in both BC-T and BC-P were analyzed by Electron Probe Micro-analyzer (EPMA) using a Cameca SX-100 electron microprobe at Oregon State University (OSU), USA, with an accelerating voltage of 15 KV and an electron beam of 30 nA. A beam size of 5 μm was used for glass analysis.

Geochronology

Sanidine phenocrysts were separated at Rock Preparation Lab of OSU. Raw samples were gently and coarsely crushed with hammer to avoid damage to single large crystals, and then phenocrysts like feldspar and quartz were separated from crushed granules using 1.5 Amps magnetism with Frantz Isodynamic Separator. The non-magnetic phenocrysts were etched for 8 minutes in 15% hydrofluoric acid in an ultrasonic bath to remove melt inclusion and adhering glass. Magnetic separation and hydrofluoric acid etching were repeated progressively until the crystals became purity and free of visible impurities and melt inclusion. Next, the alkali feldspar was extracted from non-magnetic clean crystals using Heavy Liquid Separator in 2.582 g/cm^3. Then, the large sanidine crystals (>850 μm) were sieved for the single-crystal step-heating fuse. Finally, each

piece of alkali feldspar was handpicked to remove the crystal remaining any impurities under a binocular microscope.

Prepared crystals were split into ~100 mg aliquots, wrapped in aluminum foil, and loaded into quartz tubes of 5 mm in diameter and ~10 cm in length. International standard Fish Canyon Tuff sanidine (FCT) with an age of 28.201 ± 0.023 Ma (Kuiper et al., 2008) was loaded within wells adjacent to the samples and throughout the entire stack to permit detailed characterization of the irradiation flux to the samples. They were then irradiated for 1 h at OSU TRIGA reactor in the Cadmium-Lined In-Core Irradiation Tube. Argon extraction for heating was performed using a 25 W Synrad CO_2 laser with industrial scan head at OSU Argon Geochronology Lab. The purified gas was analyzed on an ARGUS VI multi-collector mass spectrometer with five fixed Faraday detectors and one ion-counting CuBe electron multiplier mounted detector.

All resulting ages are calculated using the ArArCALC v2.7.2 software package (Koppers, 2002). Uncertainties reflect ± 2σ analytical contributions. In addition, the J values used in the age calculation were configured according to the position of sample aliquots in the quartz tube and TRIGA reactor. For each sample, we report $^{40}Ar/^{39}Ar$ dating results that show a relatively younger weighted plateau age with more released ^{39}Ar gas (>90%) and smaller MSWD value (than those presented in Table S2). To justify such criteria for the selection of the reported younger ages, we applied the same analytical protocol to date both the Millennium eruption (~1.1 ka or 946-947 CE; Xu et al., 2013) and Qixiangzhan eruption (~8.1 cal ^{14}C ka; Sun et al., 2018) of the CBS-TC volcano. The relatively younger plateau ages obtained for these two recent eruptions are 1.1 ± 0.8 ka and 8.2 ± 1.3 ka, respectively, in good agreement with their corresponding radiocarbon-dated eruption ages (Pan et al., 2020). This finding indicates that the younger end of the plateau ages derived for each sample most likely approximates the actual eruption age, and other relatively older ages might have been influenced by excess argon in the samples. The sources of excess argon will be discussed in a separate paper.

SUPPLEMENTARY FIGURES

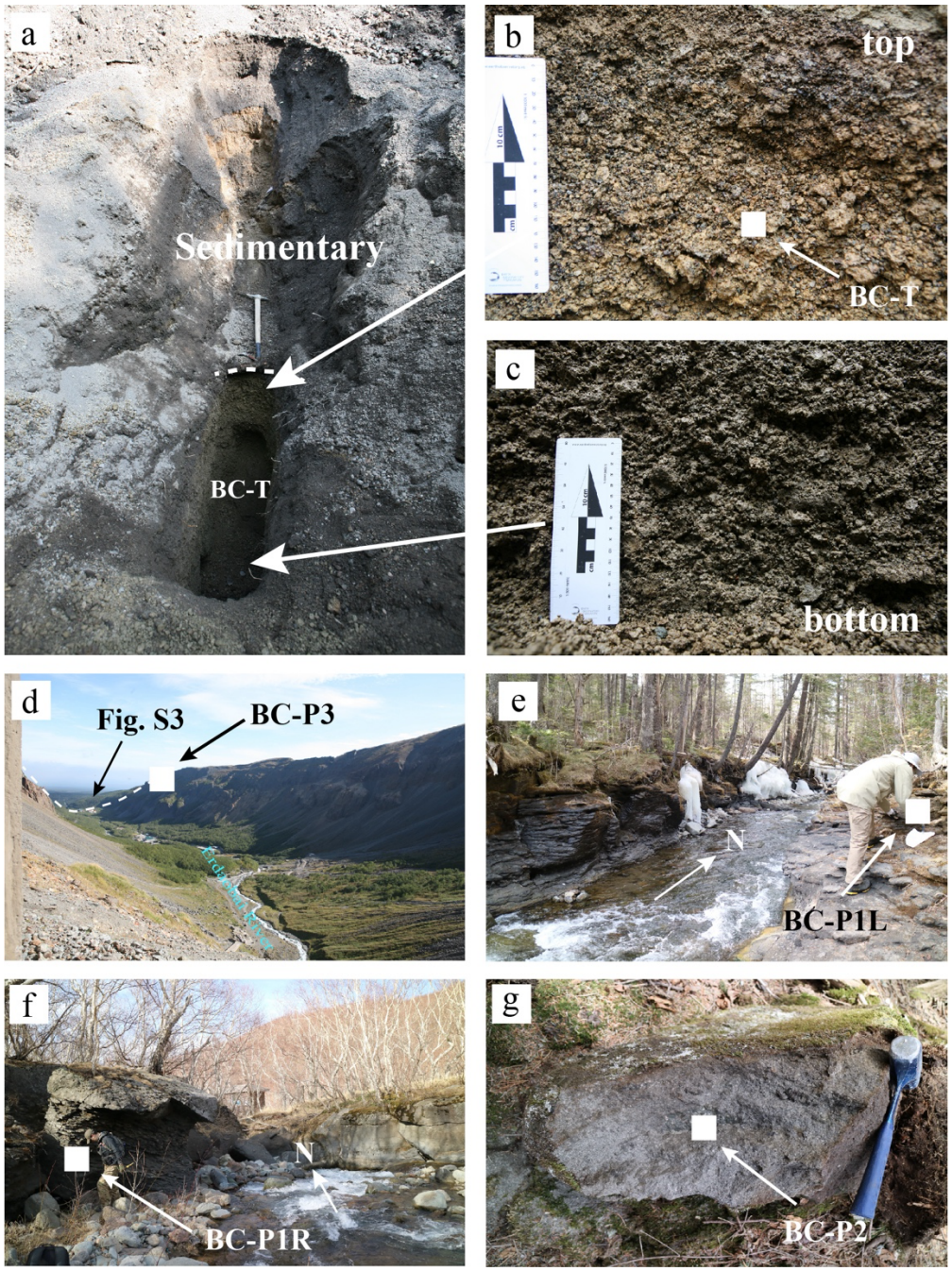

Figure S1. Field photos showing the BC tephra deposit (BC-T) in Heishi Valley (HSV) and BC pyroclastic deposit (BC-P) in the Erdaobai Valley (EBV). (a) A trench in HSV fully exposing the BC-T deposit. (b) Light-yellow tephra at the top section of the BC-T deposit. (c) Grey tephra at the bottom section of the BC-T depoist. (d) BC-P deposits in EBV viewed northward from the Tianchi water fall. (e) BC-P deposit along EBV at the coach transfer station. (f) BC-P deposit along EBV at the Xiaotianchi pond. (g) Close-up view of a rock sample (BC-P2).

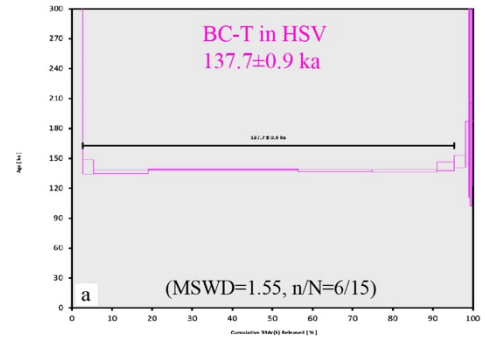
BC-T in HSV
137.7±0.9 ka
(MSWD=1.55, n/N=6/15)
a

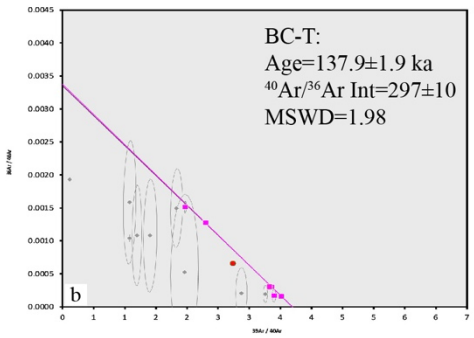
BC-T:
Age=137.9±1.9 ka
40Ar/36Ar Int=297±10
MSWD=1.98
b

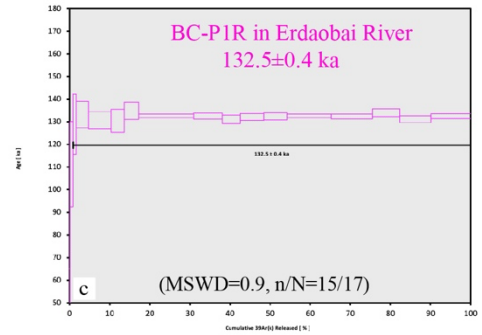
BC-P1R in Erdaobai River
132.5±0.4 ka
(MSWD=0.9, n/N=15/17)
c

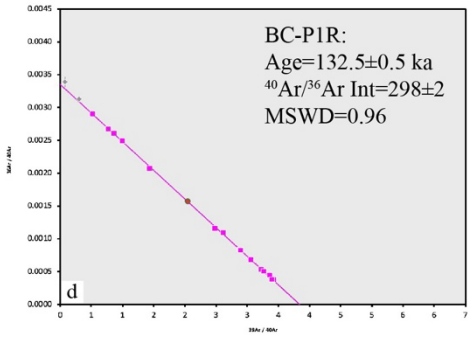
BC-P1R:
Age=132.5±0.5 ka
40Ar/36Ar Int=298±2
MSWD=0.96
d

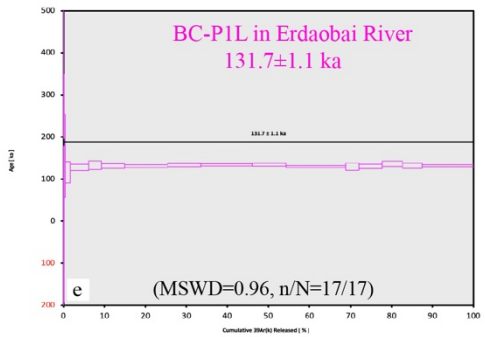
BC-P1L in Erdaobai River
131.7±1.1 ka
(MSWD=0.96, n/N=17/17)
e

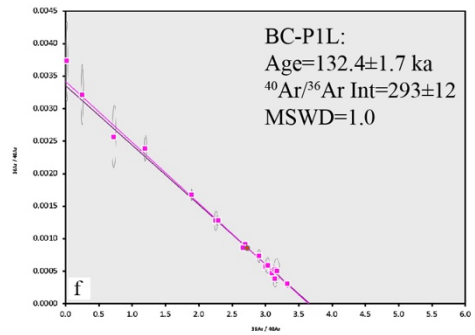
BC-P1L:
Age=132.4±1.7 ka
40Ar/36Ar Int=293±12
MSWD=1.0
f

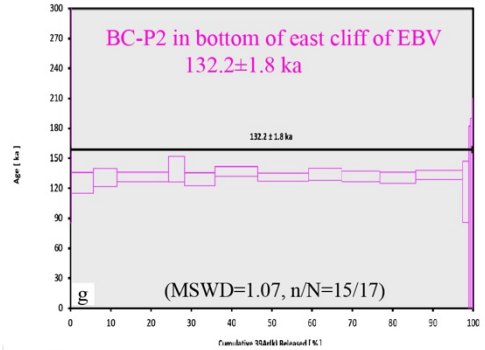
BC-P2 in bottom of east cliff of EBV
132.2±1.8 ka
(MSWD=1.07, n/N=15/17)
g

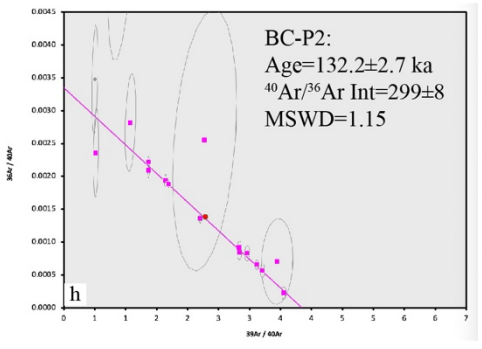
BC-P2:
Age=132.2±2.7 ka
40Ar/36Ar Int=299±8
MSWD=1.15
h

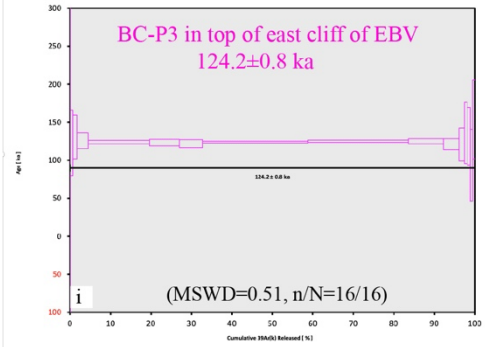
BC-P3 in top of east cliff of EBV
124.2±0.8 ka
(MSWD=0.51, n/N=16/16)
i

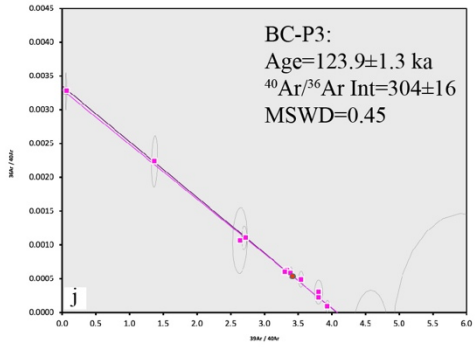
BC-P3:
Age=123.9±1.3 ka
40Ar/36Ar Int=304±16
MSWD=0.45
j

Figure S2. $^{40}Ar/^{39}Ar$ plateau age spectra and inverse isochron plots of the single-crystal incremental heating with 15-17 steps for 5 samples of the BC eruptions. Sample locations are given in Table 1 and Figures 1 and 3. All age data are reported with 2-sigma uncertainties. Purple steps are used in plateau age calculation while grey steps are not. Red dots denote total fusion ages for each sample. MSWD is mean square of weighted deviates, n is the number of heating steps used in plateau age calculation, and N is the total number of heating steps used in $^{40}Ar/^{39}Ar$ age measurements. (a, b) BC tephra in HSV, first deposited in the BC eruption episode and yielded the oldest plateau age (137.7 ± 0.9 ka) among 5 samples. (c, d) BC tuff, sampled on the right bank of EBV and produced during the middle session of the BC eruption episode. (e, f) BC tuff, sampled on the left bank of EBV and produced during the middle session of the BC eruption episode. (g, h) BC tuff, sampled at the bottom of east cliff along EBV. (i, j) BC tuff, sampled on the top of east cliff along EBV.

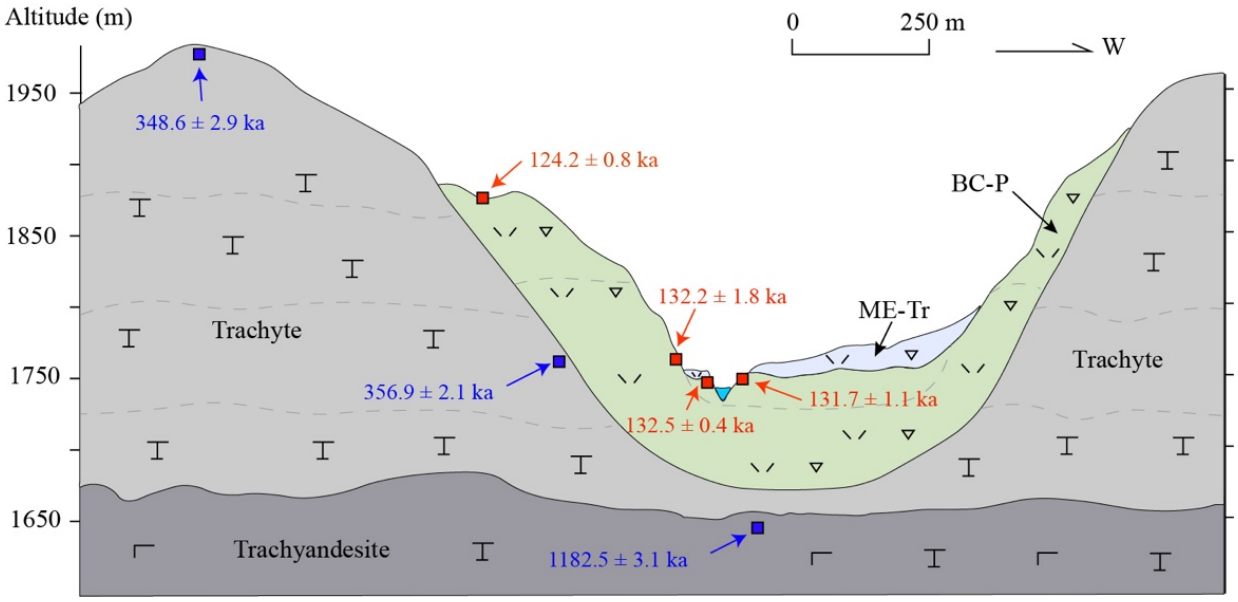

Figure S3. Cross-sectional distribution of volcanic deposits at EBV, showing BC pyroclastic flow sequences and relevant $^{40}Ar/^{39}Ar$ ages, along with ME-Tr deposits produced in 946-947 CE (Pan et al., 2020). The surrounding rock is trachyte emplaced during the cone-forming stage around 1.18-0.35 Ma.

References

Koppers, A. A. P. (2002). ArArCALC-software for $^{40}Ar/^{39}Ar$ age calculations. *Computers & Geosciences, 28*, 605-619.

Kuiper, K. F., Deino, A., Hilgen, F. J., Krijgsman, W., Renne, P. R., & Wijbrans, J. R. (2008). Synchronizing Rock Clocks of Earth History. *Science, 320,* 500-504.

Pan, B., de Silva, S. L., Xu, J. D., Liu, S. J., & Xu, D. (2020). Late Pleistocene to present day eruptive history of the Changbaishan-Tianchi Volcano, China/DPRK: New field, geochronological and chemical constraints. *Journal of Volcanology and Geothermal Research, 399,* L106870.

Sun, C. Q., Wang, L., Plunkett, G., You, H. T., Zhu, Z. Y., Zhang, L., et al. (2018). Ash from the Changbaishan Qixiangzhan Eruption: A new early Holocene marker horizon across East Asia. *Journal of Geophysical Research - Solid Earth, 123*, 6442-6450.

Xu, J. D., Pan, B., Liu, T. Z., Hajdas, I., Zhao, B., Yu, H. M., et al. (2013). Climatic impact of the Millennium eruption of Changbaishan volcano in China: new insights from high-precision radiocarbon wiggle-match dating. *Geophysical Research Letters, 40,* 54–59.

Table S1. GEOCHEMISTRY RESULTS (major elements by EPMA)

Deposit Unit	Sample	SiO[2]	TiO[2]	Al[2]O[3]	FeO	MnO	MgO	CaO	Na[2]O	K[2]O
ME-Tr	LA-20	65.719	0.735	15.717	6.136	0.173	0.208	1.305	3.899	5.897
ME-Tr	LA-20	65.771	0.538	16.767	5.103	0.073	0.261	1.42	4.003	5.846
ME-Tr	LA-20	66.238	0.526	16.75	5.047	0.17	0.247	1.419	3.28	6.077
ME-Tr	LA-20	66.574	0.504	16.467	5.102	0.128	0.215	1.388	3.916	5.469
ME-Tr	LA-20	66.059	0.562	16.373	5.021	0.141	0.281	1.499	4.236	5.577
ME-Tr	17 thin_1	65.476	0.479	16.425	5.274	0.178	0.188	1.469	4.791	5.507
ME-Tr	17 thin_1	65.243	0.49	16.452	5.252	0.125	0.196	1.52	4.801	5.687
ME-Tr	17 thin_1	65.498	0.476	16.251	5.174	0.153	0.197	1.538	4.844	5.629
ME-Tr	17 thin_1	65.382	0.46	16.452	5.133	0.142	0.188	1.35	4.691	5.99
ME-Tr	17 thin_1	65.386	0.452	16.25	5.044	0.127	0.189	1.715	4.904	5.699
ME-Tr	17 thin_2	66.091	0.477	16.509	5.155	0.185	0.188	1.083	3.866	6.254
ME-Tr	17 thin_2	65.53	0.481	16.593	4.873	0.138	0.193	1.242	4.657	6.106
ME-Tr	17 thin_2	65.761	0.463	16.331	5.007	0.129	0.189	1.711	4.665	5.535
ME-Tr	17 thin_2	65.28	0.47	16.461	5.151	0.191	0.185	1.352	4.915	5.796
ME-Tr	17 thin_2	65.751	0.487	16.582	4.89	0.121	0.181	1.118	4.828	5.845
ME-Tr	LA-04_01	65.303	0.464	16.425	5.158	0.124	0.213	1.332	4.92	5.86
ME-Tr	LA-04_01	65.008	0.517	16.587	5.216	0.13	0.245	1.463	4.861	5.759
ME-Tr	LA-04_01	65.136	0.521	16.893	5.203	0.11	0.247	1.487	4.308	5.89
ME-Tr	LA-04_01	65.204	0.503	16.746	5.173	0.148	0.238	1.462	4.596	5.681
ME-Tr	LA-04_01	65.408	0.503	16.619	4.997	0.157	0.202	1.315	5.05	5.545
ME-Tr	LA-04_02	66.42	0.458	16.415	5.072	0.145	0.179	1.331	4.046	5.707
ME-Tr	LA-04_02	65.407	0.53	16.225	5.185	0.159	0.271	1.478	4.941	5.579
ME-Tr	LA-04_02	65.648	0.543	16.787	5.192	0.153	0.256	1.41	3.919	5.885
ME-Tr	LA-03	65.949	0.479	15.847	5.04	0.138	0.211	1.15	4.762	6.198
ME-Tr	LA-03	65.748	0.477	15.868	5.133	0.14	0.182	1.346	6.532	4.364
ME-Tr	LA-03	66.132	0.511	15.799	5.049	0.129	0.269	1.095	5.164	5.628
ME-Tr	LA-03	65.66	0.512	16.216	5.212	0.124	0.283	1.569	4.371	5.825
ME-Tr	LA-05	65.581	0.462	15.998	5.162	0.168	0.192	1.279	5.112	5.847
ME-Tr	LA-05	66.13	0.462	15.764	5.108	0.14	0.191	1.286	5.095	5.619
ME-Tr	LA-05	65.562	0.462	16.11	5.113	0.111	0.183	1.321	5.382	5.549
ME-Tr	LA-05	66.028	0.474	15.891	5.05	0.121	0.195	1.278	4.86	5.906
ME-Tr	LA-05	65.474	0.465	16.014	5.177	0.179	0.198	1.269	5.209	5.811
ME-Tr	LA-05	64.995	0.517	16.78	5.021	0.097	0.244	1.425	5.099	5.603
ME-com	LA-10	74.9	0.238	10.976	4.184	0.059	0.012	0.207	4.561	4.381
ME-com	LA-10	75.055	0.209	10.869	4.251	0.079	0.016	0.241	4.528	4.261
ME-com	LA-10	74.924	0.234	10.992	4.239	0.09	0.019	0.216	4.3	4.515

ME-com	LA-10	75.182	0.227	10.81	4.286	0.097	0.025	0.231	4.223	4.44
ME-com	LA-10	74.593	0.221	11.009	4.307	0.036	0.018	0.228	4.759	4.344
ME-com	LA-10	75.133	0.245	10.959	4.251	0.112	0.012	0.216	4.232	4.366
ME-com	LA-10	75.011	0.235	10.868	4.178	0.09	0.017	0.207	4.596	4.314
ME-com	LA-10	74.902	0.215	11.078	4.248	0.055	0.012	0.223	4.355	4.416
ME-com	LA_19_sample	74.952	0.253	11.566	4.371	0.088	0.026	0.308	3.436	4.536
ME-com	LA_19_sample	74.898	0.263	11.539	4.38	0.072	0.027	0.313	3.304	4.663
ME-com	LA_19_sample	74.866	0.263	11.747	4.455	0.109	0.02	0.344	3.029	4.716
ME-com	LA_19_sample	75.616	0.222	11.347	4.275	0.064	0.016	0.261	3.311	4.405
ME-com	LA_19_sample	75.457	0.27	11.825	4.517	0.042	0.033	0.324	2.269	4.783
ME-com	LA_19_sample	75.953	0.257	11.607	4.312	0.097	0.016	0.303	2.279	4.712
BKY-1	BKY1	75.14	0.23	9.17	5.91	0.12	0	0.22	5.02	4.18
BKY-1	BKY2	75.08	0.15	9.39	6	0.11	0	0.21	4.83	4.24
BKY-1	BKY3	73.88	0.1	10.51	5.79	0.15	0	0.35	4.71	4.5
BKY-1	BKY4	72.41	0.03	11.86	5.48	0.13	0	0.48	5.21	4.4
BKY-1	BKY5	73.69	0.16	11.53	5.61	0.15	0	0.44	3.9	4.5
BKY-1	BKY6	70.6	0.15	13.28	5.2	0.15	0.02	0.62	5.38	4.6
BKY-1	BKY7	73.26	0.07	11.26	6.05	0.14	0	0.63	4.23	4.36
BKY-1	BKY8	74.96	0.22	9.24	5.81	0.13	0.04	0.24	5.06	4.29
BKY-1	BKY9	75.36	0.12	9.2	5.75	0.13	0	0.22	4.9	4.32
BKY-1	BKY10	67.53	0.22	15.15	5.3	0.16	0.09	1	5.34	5.21
BKY-1	BKY11	68.63	0.2	15.5	5.44	0.14	0.09	0.97	3.67	5.35
BKY-1	BKY12	68.47	0.27	15.06	5.37	0.19	0.05	0.89	4.37	5.32
BKY-1	BKY13	66.59	0.16	15.74	5.54	0.15	0.08	1.09	5.47	5.17
BKY-1	BKY14	67.68	0.22	15.76	5.45	0.13	0.12	1.06	4.3	5.29
BKY-1	BKYT	68.45	0.17	14.7	5.2	0.17	0.05	0.9	5.33	5.05
BC-P2	LYT1-01	67.38	0.02	15.92	3.47	0.01	0.00	0.00	5.89	7.32
BC-P2	LYT1-4	73.12	0.08	12.52	3.43	0.05	0.00	0.05	4.74	6.01
BC-P2	LYT1-5	75.57	0.03	12.14	2.55	0.00	0.00	0.00	4.23	5.48
BC-P2	LYT1-6	76.30	0.03	11.39	2.73	0.01	0.00	0.00	4.46	5.09
BC-P2	LYT1-7	78.20	0.07	10.59	2.35	0.03	0.00	0.02	3.82	4.93
BC-P2	LYT1-10	69.08	0.05	16.13	2.37	0.03	0.01	0.05	5.84	6.43
BC-P2	LYT1-12	73.53	0.03	12.96	2.60	0.00	0.00	0.02	4.96	5.90
BC-P2	LYT1-13	67.68	0.04	16.18	2.93	0.00	0.00	0.01	6.08	7.08
BC-P2	LYT1-16	68.73	0.03	15.54	2.93	0.02	0.00	0.00	5.70	7.05
BC-P2	LYT1-17	75.50	0.06	11.79	2.88	0.03	0.01	0.02	4.57	5.15
BC-P2	LYT1-18	74.91	0.02	12.00	2.64	0.04	0.00	0.00	5.13	5.27
BC-P2	LYT1-19	70.36	0.01	15.16	2.33	0.02	0.00	0.00	5.78	6.35
BC-P2	LYT1-21	74.48	0.03	12.41	2.70	0.01	0.00	0.00	4.86	5.51

BC-P2	**LYT1-23**	**75.92**	**0.04**	**11.38**	**2.81**	**0.04**	**0.00**	**0.02**	**4.42**	**5.38**
BC-P2	**LYT1-24**	**70.20**	**0.02**	**14.62**	**3.08**	**0.01**	**0.00**	**0.17**	**5.99**	**5.91**
BC-P2	**LYT1-25**	**68.52**	**0.35**	**14.31**	**4.72**	**0.12**	**0.11**	**0.89**	**6.74**	**4.25**
BC-P2	**LYT1-26**	**67.75**	**0.40**	**14.73**	**4.83**	**0.12**	**0.11**	**0.95**	**6.74**	**4.37**
BC-P2	**LYT1-27**	**72.98**	**0.20**	**12.02**	**4.00**	**0.18**	**0.02**	**0.12**	**5.09**	**5.40**
BC-P2	**LYT1-29**	**67.46**	**0.01**	**15.74**	**3.70**	**0.02**	**0.00**	**0.05**	**5.91**	**7.11**
BC-P2	**LYT1-30**	**72.27**	**0.08**	**13.95**	**2.52**	**0.01**	**0.00**	**0.03**	**5.55**	**5.59**
BC-P2	**LYT1-31**	**69.75**	**0.08**	**14.06**	**4.00**	**0.04**	**0.05**	**0.68**	**5.34**	**6.00**
BC-P2	**LYT1-32**	**67.40**	**0.28**	**15.82**	**3.76**	**0.02**	**0.00**	**0.01**	**5.71**	**7.01**
BC-P2	**LYT1-33**	**70.93**	**0.06**	**14.23**	**2.96**	**0.04**	**0.00**	**0.01**	**5.30**	**6.47**
BC-P2	**LYT1-35**	**73.49**	**0.04**	**12.93**	**2.59**	**0.01**	**0.00**	**0.02**	**4.92**	**6.01**
BC-P2	**LYT3-1**	**67.95**	**0.34**	**14.65**	**4.32**	**0.10**	**0.05**	**0.80**	**5.77**	**6.01**
BC-P2	**LYT3-3**	**67.22**	**0.33**	**14.79**	**4.80**	**0.14**	**0.10**	**1.00**	**5.63**	**5.98**
BC-P2	**LYT3-4**	**66.91**	**0.24**	**16.86**	**2.98**	**0.01**	**0.00**	**0.35**	**6.67**	**5.99**
BC-P2	**LYT3-5**	**71.80**	**0.11**	**13.12**	**3.78**	**0.10**	**0.10**	**0.85**	**4.81**	**5.32**
BC-P2	**LYT3-7**	**71.55**	**0.16**	**14.42**	**2.59**	**0.01**	**0.00**	**0.07**	**5.10**	**6.09**
BC-P2	**LYT3-8**	**67.87**	**0.38**	**14.92**	**4.68**	**0.03**	**0.00**	**0.08**	**5.71**	**6.33**
BC-P2	**LYT3-10**	**68.21**	**0.06**	**16.50**	**2.29**	**0.00**	**0.00**	**0.04**	**6.33**	**6.57**
BC-P2	**LYT3-11**	**74.72**	**0.15**	**12.29**	**2.58**	**0.02**	**0.01**	**0.20**	**4.46**	**5.57**
BC-P2	**LYT3-12**	**68.03**	**0.03**	**16.58**	**2.47**	**0.00**	**0.00**	**0.02**	**6.40**	**6.48**
BC-P2	**LYT3-13**	**67.29**	**0.08**	**16.13**	**3.03**	**0.05**	**0.01**	**0.31**	**6.76**	**6.34**
BC-P2	**LYT3-14**	**73.00**	**0.12**	**13.16**	**3.00**	**0.00**	**0.00**	**0.01**	**5.13**	**5.58**
BC-P2	**LYT3-4**	**75.30**	**0.07**	**12.52**	**2.12**	**0.00**	**0.00**	**0.11**	**4.53**	**5.36**
BC-P2	**LYT32-1**	**68.53**	**0.37**	**14.26**	**4.62**	**0.11**	**0.11**	**0.91**	**6.64**	**4.45**
BC-P2	**LYT32-3**	**68.67**	**0.42**	**13.95**	**5.04**	**0.07**	**0.07**	**0.70**	**5.32**	**5.75**
BC-P2	**LYT32-4**	**68.38**	**0.01**	**16.35**	**2.35**	**0.01**	**0.00**	**0.04**	**5.74**	**7.12**
BC-P2	**LYT32-5**	**67.20**	**0.32**	**15.19**	**4.84**	**0.16**	**0.06**	**1.17**	**5.82**	**5.24**
BC-P2	**LYT32-6**	**67.99**	**0.33**	**14.50**	**4.65**	**0.09**	**0.14**	**0.88**	**6.21**	**5.22**
BC-P2	**LYT12-2**	**67.85**	**0.02**	**16.34**	**2.73**	**0.00**	**0.00**	**0.01**	**6.22**	**6.83**
BC-P2	**LYT12-3**	**74.89**	**0.07**	**11.90**	**3.05**	**0.01**	**0.01**	**0.02**	**4.43**	**5.62**
BC-P2	**LYT12-4**	**68.46**	**0.33**	**14.23**	**4.90**	**0.13**	**0.06**	**0.91**	**6.86**	**4.11**
BC-P2	**LYT12-5**	**75.41**	**0.01**	**11.92**	**2.62**	**0.01**	**0.00**	**0.00**	**4.67**	**5.36**
BC-P2	**LYT12-6**	**68.24**	**0.00**	**16.26**	**2.49**	**0.02**	**0.00**	**0.00**	**5.74**	**7.25**
BC-P2	**LYT12-7**	**76.28**	**0.07**	**11.62**	**2.54**	**0.01**	**0.01**	**0.02**	**4.42**	**5.04**
BC-P2	**LYT12-8**	**69.02**	**0.06**	**14.85**	**3.50**	**0.04**	**0.00**	**0.00**	**5.87**	**6.66**
BC-P2	**LYT12-9**	**67.00**	**0.45**	**16.61**	**3.15**	**0.05**	**0.06**	**0.39**	**6.26**	**6.04**
BC-P2	**LYT12-10**	**68.31**	**0.04**	**15.05**	**3.66**	**0.00**	**0.00**	**0.00**	**5.84**	**7.10**
BC-P1	**DXTF glass**	**67.27**	**0.14**	**15.36**	**3.82**	**0.16**	**0.06**	**0.93**	**6.51**	**5.75**
BC-P1	**DXTF glass**	**65.15**	**0.54**	**15.78**	**4.59**	**0.17**	**0.25**	**1.28**	**5.91**	**6.34**

BC-P1	**CTL1 glass**	**65.43**	**0.46**	**16.85**	**3.54**	**0.10**	**0.21**	**0.83**	**6.34**	**6.23**
BC-P1	**BCC1 glass**	**66.26**	**0.50**	**15.17**	**5.17**	**0.16**	**0.22**	**1.24**	**6.29**	**4.98**
BC-P1	**BCC1 glass**	**65.90**	**0.55**	**15.04**	**5.47**	**0.08**	**0.23**	**1.41**	**6.42**	**4.90**
BC-P1	**BCC1 glass**	**71.03**	**0.40**	**13.07**	**4.41**	**0.10**	**0.11**	**0.93**	**4.70**	**5.25**
BC-P1	**BCL1 Glass**	**69.03**	**0.14**	**15.89**	**2.56**	**0.06**	**0.01**	**0.20**	**6.45**	**5.65**
BC-P1	**BCL1 Glass**	**68.65**	**0.25**	**16.00**	**2.52**	**0.05**	**0.02**	**0.19**	**6.23**	**6.10**
BC-P1	**BCL1 Glass**	**67.54**	**0.27**	**16.10**	**3.54**	**0.08**	**0.07**	**0.64**	**6.14**	**5.62**
BC-P1	**BCL1 Glass**	**66.44**	**0.33**	**15.50**	**4.21**	**0.19**	**0.09**	**1.16**	**5.89**	**6.21**
BC-P1	**BCL1 Glass**	**66.41**	**0.47**	**15.17**	**4.71**	**0.10**	**0.16**	**1.15**	**5.71**	**6.12**
BC-P1	**BCL1 Glass**	**66.66**	**0.35**	**15.21**	**5.01**	**0.09**	**0.10**	**0.91**	**6.03**	**5.65**
BC-P1	**BCR1 Glass**	**69.53**	**0.03**	**14.16**	**3.74**	**0.01**	**0.01**	**0.01**	**5.48**	**7.02**
BC-P1	**BCR1 Glass**	**64.52**	**0.22**	**14.96**	**5.60**	**0.17**	**0.28**	**2.58**	**5.86**	**5.80**
BC-T	**TY03 glass**	**73.85**	**0.24**	**8.61**	**6.81**	**0.11**	**0.01**	**0.22**	**5.96**	**4.18**
BC-T	**TY03 glass**	**72.96**	**0.23**	**8.94**	**6.74**	**0.17**	**0.00**	**0.24**	**6.34**	**4.37**
BC-T	**TY03 glass**	**73.64**	**0.26**	**8.84**	**6.52**	**0.21**	**0.01**	**0.22**	**6.16**	**4.14**
BC-T	**TY03 glass**	**73.56**	**0.26**	**8.68**	**6.74**	**0.14**	**0.01**	**0.28**	**6.17**	**4.17**
BC-T	**TY03 glass**	**73.33**	**0.25**	**8.63**	**6.72**	**0.16**	**0.00**	**0.25**	**6.34**	**4.33**
BC-T	**TY03 glass**	**73.74**	**0.23**	**8.73**	**6.55**	**0.11**	**0.03**	**0.23**	**6.12**	**4.25**
BC-T	**TY03 glass**	**72.89**	**0.25**	**9.04**	**7.07**	**0.16**	**0.02**	**0.24**	**6.09**	**4.24**
BC-T	**TY03 glass**	**73.01**	**0.26**	**8.94**	**6.92**	**0.15**	**0.01**	**0.27**	**6.27**	**4.18**
BC-T	**TY03 glass**	**72.98**	**0.25**	**8.87**	**6.87**	**0.18**	**0.01**	**0.24**	**6.20**	**4.39**
BC-T	**TY03 glass**	**72.74**	**0.22**	**9.01**	**7.00**	**0.18**	**0.03**	**0.28**	**6.30**	**4.26**
B-Tm	**C01**	**74.9**	**0.24**	**10.58**	**3.92**	**0.1**	**0**	**0.23**	**5.27**	**4.26**
B-Tm	**C02**	**74.97**	**0.2**	**10.36**	**4.13**	**0.08**	**0**	**0.23**	**5.25**	**4.3**
B-Tm	**C03**	**66.15**	**0.48**	**15.49**	**4.81**	**0.17**	**0.23**	**1.25**	**5.45**	**5.76**
B-Tm	**C04**	**66.12**	**0.48**	**15.66**	**4.64**	**0.16**	**0.18**	**1.26**	**5.67**	**5.62**
B-Tm	**C05**	**66.2**	**0.42**	**15.86**	**4.35**	**0.12**	**0.17**	**1.26**	**5.81**	**5.63**
B-Tm	**SG06-0226**	**74.8447**	**0.2084**	**10.2208**	**3.9181**	**0.0605**	**0**	**0.1779**	**5.7088**	**4.4047**
B-Tm	**SG06-0226**	**75.1729**	**0.2384**	**10.1762**	**3.9513**	**0.0629**	**0.0688**	**0.2289**	**5.1934**	**4.4311**
B-Tm	**SG06-0226**	**74.8253**	**0.2569**	**10.2984**	**4.1985**	**0**	**0.0007**	**0.2328**	**5.2891**	**4.4141**
B-Tm	**SG06-0226**	**75.4878**	**0.2036**	**10.2049**	**3.7242**	**0.0842**	**0.0511**	**0.2226**	**5.0946**	**4.4401**
B-Tm	**SG06-0226**	**74.9608**	**0.178**	**10.2273**	**3.9938**	**0.1171**	**0**	**0.2168**	**5.337**	**4.4579**
B-Tm	**SG06-0226**	**74.9464**	**0.2636**	**10.1375**	**3.9703**	**0.0924**	**0.0022**	**0.2363**	**5.4312**	**4.4047**
B-Tm	**SG06-0226**	**74.8675**	**0.2946**	**10.389**	**3.9801**	**0.1251**	**0**	**0.2859**	**5.1949**	**4.3492**
B-Tm	**SG06-0226**	**75.1391**	**0.1903**	**10.1676**	**4.0212**	**0.0554**	**0.0226**	**0.231**	**5.3398**	**4.3516**
B-Tm	**SG06-0226**	**74.7322**	**0.1965**	**10.1621**	**4.1708**	**0.0907**	**0.0536**	**0.2307**	**5.3395**	**4.4787**
B-Tm	**SG06-0226**	**75.198**	**0.2274**	**10.194**	**4.1893**	**0.1125**	**0.0038**	**0.2358**	**5.1227**	**4.2228**
B-Tm	**SG06-0226**	**75.0376**	**0.169**	**10.1935**	**4.1984**	**0.092**	**0.0264**	**0.2107**	**5.2039**	**4.4115**
B-Tm	**SG06-0226**	**74.6145**	**0.2324**	**10.4898**	**4.055**	**0.1085**	**0.0207**	**0.2347**	**5.1579**	**4.5461**

B-Tm	**SG06-0226**	**74.9363**	**0.252**	**10.2458**	**4.2782**	**0.0864**	**0.0079**	**0.2096**	**5.2589**	**4.2057**
B-Tm	**SG06-0226**	**74.6685**	**0.2322**	**10.3079**	**4.1014**	**0.0377**	**0**	**0.2432**	**5.4945**	**4.43**
B-Tm	**SG06-0226**	**74.8885**	**0.2337**	**10.3178**	**3.9749**	**0.1356**	**0**	**0.2277**	**5.5121**	**4.2145**
B-Tm	**SG06-0226**	**74.5663**	**0.1867**	**10.2835**	**4.2682**	**0.0415**	**0**	**0.1793**	**5.5104**	**4.4444**
B-Tm	**SG06-0226**	**74.8024**	**0.2431**	**10.3032**	**4.2688**	**0.0412**	**0**	**0.2318**	**5.3341**	**4.2723**
B-Tm	**SG06-0226**	**75.075**	**0.1963**	**10.2353**	**4.053**	**0.0896**	**0**	**0.1881**	**5.2714**	**4.4534**
B-Tm	**SG06-0226**	**74.6534**	**0.284**	**10.2779**	**4.1859**	**0.1718**	**0.0145**	**0.1974**	**5.4154**	**4.2683**
B-Tm	**SG06-0226**	**74.8449**	**0.1917**	**10.2245**	**4.0533**	**0.0942**	**0.0337**	**0.2112**	**5.5314**	**4.3113**
B-Tm	**SG06-0226**	**74.8509**	**0.1863**	**10.5342**	**3.8961**	**0.1231**	**0**	**0.2077**	**5.3298**	**4.3796**
B-Tm	**SG06-0226**	**65.1432**	**0.574**	**16.1021**	**4.5485**	**0.1452**	**0.2845**	**1.4781**	**5.406**	**6.1452**
B-Tm	**SG06-0226**	**74.9648**	**0.1912**	**10.2236**	**3.9918**	**0.1305**	**0.0759**	**0.1851**	**5.4806**	**4.2542**
B-Tm	**SG06-0226**	**74.8855**	**0.2349**	**10.2837**	**4.0565**	**0.0593**	**0.0636**	**0.219**	**5.419**	**4.3002**
B-Tm	**SG06-0226**	**75.058**	**0.1777**	**10.1824**	**4.0244**	**0.0355**	**0**	**0.2219**	**5.4527**	**4.3269**
B-Tm	**SG06-0226**	**74.5484**	**0.2631**	**10.301**	**4.1251**	**0.17**	**0.0025**	**0.2187**	**5.3568**	**4.5044**
B-Tm	**SG06-0226**	**74.6065**	**0.2694**	**10.4335**	**3.7342**	**0.0855**	**0**	**0.2293**	**5.6241**	**4.4389**
B-Tm	**SG06-0226**	**74.7952**	**0.2346**	**10.394**	**3.9125**	**0.1077**	**0.0623**	**0.2409**	**5.4645**	**4.2699**
B-Tm	**SG06-0226**	**74.8791**	**0.1776**	**10.2324**	**4.0153**	**0**	**0.0279**	**0.228**	**5.4472**	**4.4777**
B-Tm	**SG06-0226**	**75.0575**	**0.1962**	**10.251**	**4.2014**	**0.0062**	**0.0133**	**0.207**	**5.1704**	**4.4233**

Table S2: Summary of the $^{40}Ar/^{39}Ar$ dating results for BC eruptions at Changbaishan-Tianchi volcano

No	Sample Name	Experiment Number	Material	Method	Plateau age (ka)						Inverse isochron age (ka)		
					Age ± 2σ	^{39}Ar released	K/Ca ± 2σ	MSWD	n	N	Age ± 2σ	$^{40}Ar/^{36}Ar$ Intercept ± 2σ	MSWD
1	BC-T	21G10988	Sanidine	SCIH	137.7±0.9	92.59%	435±285	1.55	6	15	137.9±1.9	296.47±10.50	1.98
2	BC-T	21G11048	Sanidine	SCIH	139.5±1.0	53.34%	12±121	1.19	11	16	138.8±2.2	332.54±100.60	1.26
3	BC-T	21G11098	Sanidine	SCIH	141.6 ±1.0	94.67%	18.6±4.3	1.04	15	16	141.8±1.1	296.34±6.51	1.08
4	BC-T	21G11128	Sanidine	SCIH	140.1±1.7	36.96%	124±153	1.19	11	16	140.1±2.8	298.97±89.18	1.34
5	BC-T	21G11158	Sanidine	SCIH	139±0.8	77.43%	39±173	0.92	10	16	138.8±1.7	318.83±110.02	1
6	BC-T	21G11238	Sanidine	SCIH	139±1.8	74.82%	62±101	1.75	12	16	123.9±13.2	296.47±1222.29	1.12
7	BC-P1R	21G10409	Sanidine	SCIH	132.5±0.4	99.19%	8.1±0.3	0.9	15	17	132.5±0.5	298.13±1.66	0.96
8	BC-P1R	21G10441	Sanidine	SCIH	136.4±1.0	80.98%	8.3±0.4	2.91	9	17	136.3±2.5	299.1±15.22	3.33
9	BC-P1R	21G10473	Sanidine	SCIH	132±1.4	82.76%	8±1.2	0.6	13	17	132.1±2.8	309.89±10.75	0.97
10	BC-P1R	21G10525	Sanidine	SCIH	130.4±1.4	58.00%	8.4±0.2	0.82	9	17	132±1.8	293.65±3.28	0.41
11	BC-P1R	21G10557	Sanidine	SCIH	136.6±1.6	71.57%	7.2±0.2	4.75	7	17	135.3±6.3	306.17±37.96	5.52
12	BC-P1R	21G10589	Sanidine	SCIH	134±0.8	67.74%	4.1±12.3	1.55	12	17	134.1±1.9	296.78±18.90	1.72
13	BC-P1R	21G10621	Sanidine	SCIH	132.3±1.0	78.94%	7.4±3.5	1.36	9	17	132.3±1.3	304.53±4.77	1.91
14	BC-P1R	21G10673	Sanidine	SCIH	133.8±1.0	99.71%	2.92±5.02	1.11	16	17	134.3±1.0	294.89±3.30	1.07
15	BC-P1L	20F18622	Sanidine	SCIH	134.4±1.0	78.51%	8.9±0.3	1.9	12	17	135±1.7	295.65±6.85	1.96
16	BC-P1L	20F18655	Sanidine	SCIH	131.4±1.6	98.65%	8.8±0.3	1.16	14	17	128.5±2.9	331.38±26.57	0.65
17	BC-P1L	20F18688	Sanidine	SCIH	131.7±1.1	100.00%	5.9±1.7	0.96	17	17	132.4±1.7	292.55±11.74	1
18	BC-P1L	20F18721	Sanidine	SCIH	136.8±2.2	97.14%	8.8±0.4	1.8	13	17	135.6±4.4	302.58±13.45	1.9
19	BC-P2	21G10108	Sanidine	SCIH	133.1±0.9	58.10%	7.6±0.2	0.68	7	17	133±8.1	299.38±66.25	0.81
20	BC-P2	21G10140	Sanidine	SCIH	134.6±0.7	80.81%	5.4±9.0	0.44	13	17	134.6±1.2	298.37±6.25	0.48
21	BC-P2	21G10172	Sanidine	SCIH	133.3±1.4	88.11%	9.1±0.8	0.91	16	17	133.4±3.6	298.5±4.71	0.99
22	BC-P2	21G10224	Sanidine	SCIH	135.8±1.2	84.69%	6.6±9.5	1.08	13	17	134.6±2.7	302.7±7.93	1.08
23	BC-P2	21G10256	Sanidine	SCIH	133.9±0.7	88.07%	8.4±4.3	0.86	15	17	134.7±1.0	292.86±5.32	0.59
24	BC-P2	21G10288	Sanidine	SCIH	134.4±1.7	58.99%	11.7±18.3	0.68	13	17	132.6±9.7	302.15±18.48	0.73
25	BC-P2	21G10320	Sanidine	SCIH	132.2±1.8	99.69%	6.1±3.0	1.07	15	17	132.2±2.7	298.59±8.37	1.15
26	BC-P2	21G10377	Sanidine	SCIH	133.5±1.7	89.38%	9.3±0.4	0.39	10	17	133.4±2.1	299.67±12.45	0.44
27	BC-P3	20F17571	Sanidine	SCIH	126.3±1.0	99.38%	37.9±2.4	2.11	13	15	126.2±1.3	276.61±11.15	2.65
28	BC-P3	20F17603	Sanidine	SCIH	125.8±1.1	82.67%	43.6±3.3	1.81	8	15	125.9±1.1	285±77.12	2.09
29	BC-P3	20F17635	Sanidine	SCIH	126±1.4	77.68%	4.6±7.5	1.12	15	16	125.9±1.6	305.16±46.67	1.05
30	BC-P3	20F17667	Sanidine	SCIH	124.2±0.8	100.00%	10.4±8.7	0.51	16	16	123.9±1.3	303.51±16.21	0.45
31	BC-P3	20F17699	Sanidine	SCIH	125.8±2.1	95.18%	33.2±5.0	1.84	11	16	124.5±2.3	305.75±7.39	1.42

SCIH: Single Crystal Incremental Heating; MSWD: Mean Square Weighted Deviation; n: the step number of age calculation; N: the total step number of determination. Note that relatively younger weighted plateau ages (marked in red) with more released ^{39}Ar gas (>90%) and smaller MSWD values are reported for each sample.